eV-TEM: transmission electron microscopy with few-eV electrons

Geelen, D.

Chapter 3

Microscopy

eV-TEM operates in an energy regime five orders of magnitude lower than conventional transmission electron microscopy where 10 keV is considered low energy [1]. In this chapter we show that we successfully use eV-TEM to image graphene and distinguish areas with different layer numbers using the contrast due to interlayer resonances. eV-TEM can also be used to image the diffraction beams resulting from the crystal structure of the sample (LEED). Graphene and graphene oxide can also be used as a carrier substrate to image nanoscale objects in transmission with low energy electrons. Since graphene is hydrophobic and graphene oxide hydrophilic, a wide variety of objects can be studied. In this chapter we demonstrate this by imaging gold nanoparticles on graphene and DNA origami on graphene oxide.

3.1 Imaging graphene with eV-TEM

Figure 3.1 shows an eV-TEM micrograph of multilayer graphene on a lacey carbon copper TEM grid (see section 2.3) with 2.1 eV electrons, with a field of view of approximately 50 μm. The micrograph shows many regions of different brightness. This contrast is a manifestation of electron quantum interferences caused by the graphene layers, as explained in chapter 1. In chapter 4 we study the energy dependence of this contrast, which depends nontrivially

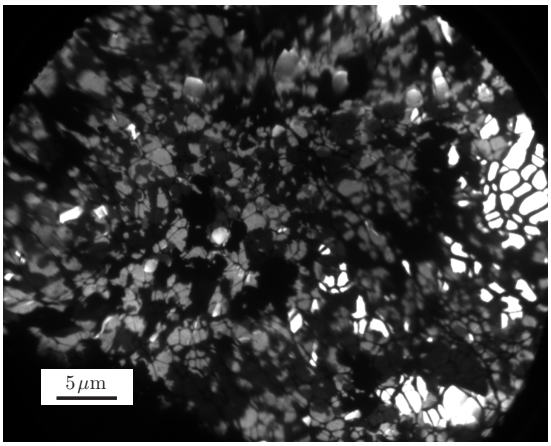

Figure 3.1: eV-TEM micrograph of freestanding multilayer graphene with an electron energy of 2.1 eV. Regions of different thickness appear with different intensities.

on the graphene layer number. The web-like structure superimposed on the graphene is the lacey carbon used to support the graphene over the $50\ \mu$m openings in the TEM grid. Furthermore, the very bright regions in the right of the image correspond to holes in the graphene. Such holes can be used to determine the incident electron current with which the graphene is illuminated. In appendix E it is explained how this is used to normalize the transmission signal.

Figure 3.2 shows a zoomed-in region on a similar sample. Here too, multilayer graphene with regions of various layer numbers can be identified from the contrast between these regions. The dark patches are regions consisting of many graphene layers through which very few electrons are transmitted. Since the graphene (multi)layer is not entirely flat and somewhat wrinkled, alignment of these Cu-grid supported samples is time consuming and cumbersome.

Therefore, we transfer the graphene with lacey carbon on the standard grids to PtPd-coated Si_3N_4 membrane with $2.5\ \mu$m diameter holes (section 2.3.1). An eV-TEM micrograph of such a sample with a large field of view is shown in figure 3.3a. This shows large regions of monolayer graphene* and several regions with multiple layers. Electrons are only transmitted through the free-

*In chapter 4 we explain how the layer number can be obtained from measurements of the energy dependent reflectivity and transmissivity.

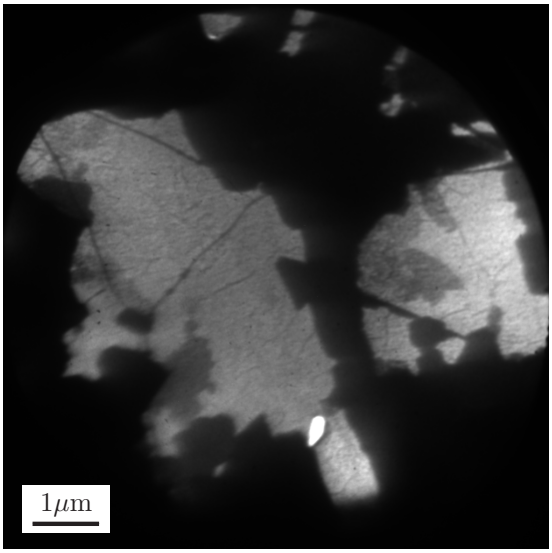

Figure 3.2: eV-TEM micrograph, measured in a bright field imaging configuration, at 3.4 eV of a smaller region on a sample similar to the one presented in figure 3.1. Here too, regions of different layer thickness can be identified from the contrast due to the interlayer resonances. Some regions have a thickness of many layers and transmit very few electrons. Such regions appear dark in the micrograph.

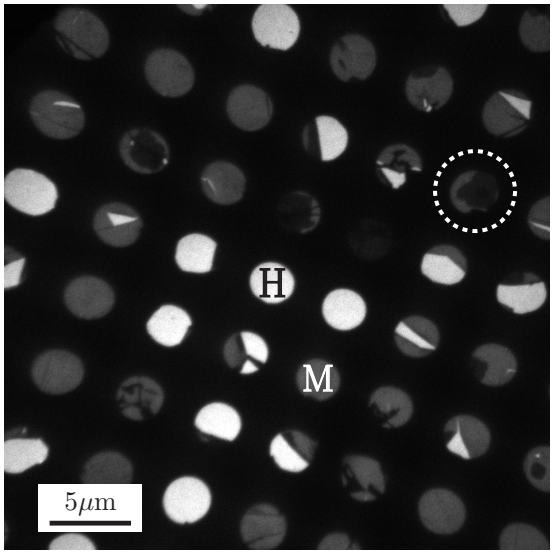

(a)

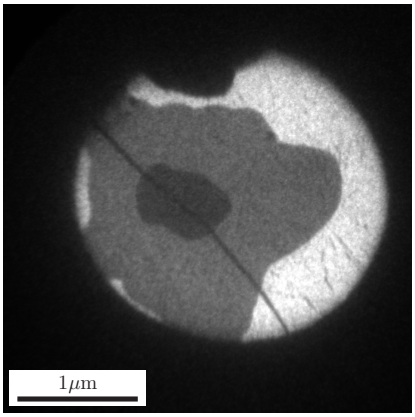

(b) eV-TEM

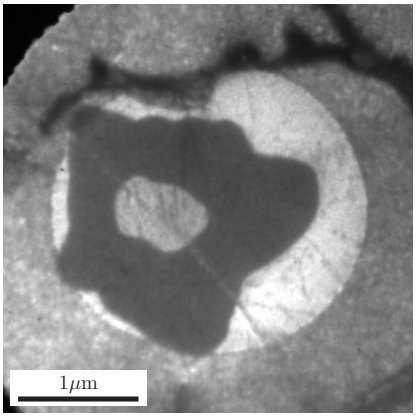

(c) LEEM

Figure 3.3: Energy-filtered eV-TEM micrographs of graphene grown on copper by CVD transferred to PtPd-coated Si_3N_4 (see section 2.3.1). **(a)** Shows a zoomed-out micrograph with 10.9 eV electrons. This reveals many holes covered by graphene. Many holes are covered by monolayer graphene. One of them is indicated with a white M. Some holes are not covered by graphene at all and can be used for the normalization of the eV-TEM signal, as explained in appendix E. One of these holes is indicated with a black H. Other holes are covered by regions of different thickness. One of them is indicated by a white dashed circle. A zoomed-in micrograph of this region is presented in **(b)**. **(c)** shows the same region obtained in reflection at 2.3 eV.

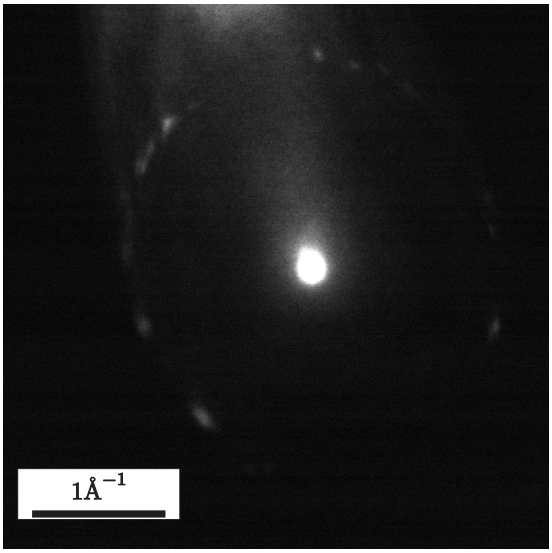

Figure 3.4: eV-TEM diffraction pattern from the region in 3.3b which was selected by selected area apertures, obtained with an electron energy of 56eV. The $(0\,0)$-spot shows the small angular spread of the transmitted electron beam. The graphene is also clean enough for diffraction spots to form.

standing suspended graphene. Outside the circular openings in the membrane, the image is dark because the coated membrane is too thick for electrons to be transmitted. Some of the circular openings in the membrane are not covered with graphene and are ideal for the normalization of the eV-TEM measurements. These openings appear much brighter than the graphene covered holes. A zoomed-in transmission micrograph of the region marked with the dashed white circle in figure 3.3a is shown in 3.3b. This is a graphene covered hole with several layer thicknesses. The same region as in 3.3b is shown in reflection in 3.3c. Only the illumination source is changed without adjusting the alignment of the imaging system. In chapter 5 we explain how the reflected and transmitted data can be combined to study the inelastic and elastic effects. In the reflection micrograph, the suspended graphene can be easily distinguished as it appears much brighter than the supported graphene. This phenomenon was studied by Locatelli et al. [2]. They find that the contrast between supported and suspended regions is related to a difference in surface roughness. Due to the absence of surface interactions with the substrate, the suspended graphene is smoother and scatters the reflected beam over a smaller angular region. As the contrast aperture cuts off electrons at larger angles, the smooth surface appears brighter than the rougher surface. In addition, the reflected intensity of graphene on the substrate is generally not expected to be the same as that of freestanding graphene as electron interference between the graphene layer and the substrate surface also plays a role.

Figure 3.4 shows the transmission diffraction pattern of the graphene region shown in 3.3b. Since the whole sample is illuminated, selected area apertures in the diagonals of the prism have been used to only select the region shown in the real space micrograph (see section 2.1.4). The pattern is obtained with a relatively high electron energy of 56 eV, which is sufficiently high for first-order diffracted beams to form (this happens at 33.1 eV). Since diffraction spots are visible, we know that the coherence length of the incident electron beam is at least as large as a few times the lattice constant of graphene (2.5 Å). From equation B.5 in appendix B we find that with the eV-TEM energy spread of 0.8 eV and at an electron energy of 56 eV the coherence length of the incoming electron beam is ~ 23 nm. Since the width of the diffraction spots is a factor ~ 10 smaller than the distance between the $(0, 0)$ and $(1, 0)$ spots we know

that the coherence length is at least a factor 10 larger than the lattice constant of graphene. This gives a lower limit to the coherence length because the diffraction spot-width is also influenced by surface roughness, quasi elastic scattering, etc.

3.2 Imaging nanoscale objects with eV-TEM

eV-TEM can also be used to image objects other than two-dimensional materials. Two-dimensional materials can be utilized as substrates for nanoscale objects. To image gold nanoparticles and DNA origami in transmission with low-energy electrons, we deposit them on graphene and graphene oxide. This allows us to show that these two-dimensional materials can indeed be used as a substrate and that eV-TEM can be applied to measure the low-energy electron transmissivity and reflectivity of individual (biological) objects. Since we used both hydrophilic and hydrophobic substrates, eV-TEM can be applied to a wide variety of organic and inorganic nanomaterials.

3.2.1 Gold nanoparticles

To demonstrate the use of graphene as a substrate for nanoscale objects we image gold nanoparticles on graphene in both reflection and transmission. After the nanoparticle suspension was applied to the sample and allowed to dry, the sample was inserted in the ESCHER setup. Immediately after this, proper imaging was impossible. The transmissivity was too low for alignment and in reflection the sample could not be properly imaged. We think this was due to sample contamination as heating the sample to ~ 440°C caused the pressure in the sample chamber to rise by about an order of magnitude. When the pressure dropped to the same value as before heating (this took about 90 min), we let the sample cool down back to room temperature. After this procedure we were able to image the sample. Figure 3.5 shows transmission and reflection micrographs of several nanoparticles on a multilayer graphene substrate (the graphene is suspended on a molybdenum coated Si_3N_4 window). In figures 3.5a and 3.5b the nanoparticles can be seen as dark spots (indicated with arrows). Line scans of these spot are presented in figures 3.5c-3.5h. Scans 1 and 2 correspond to particles on the sample. Scan 3 only shows a feature in

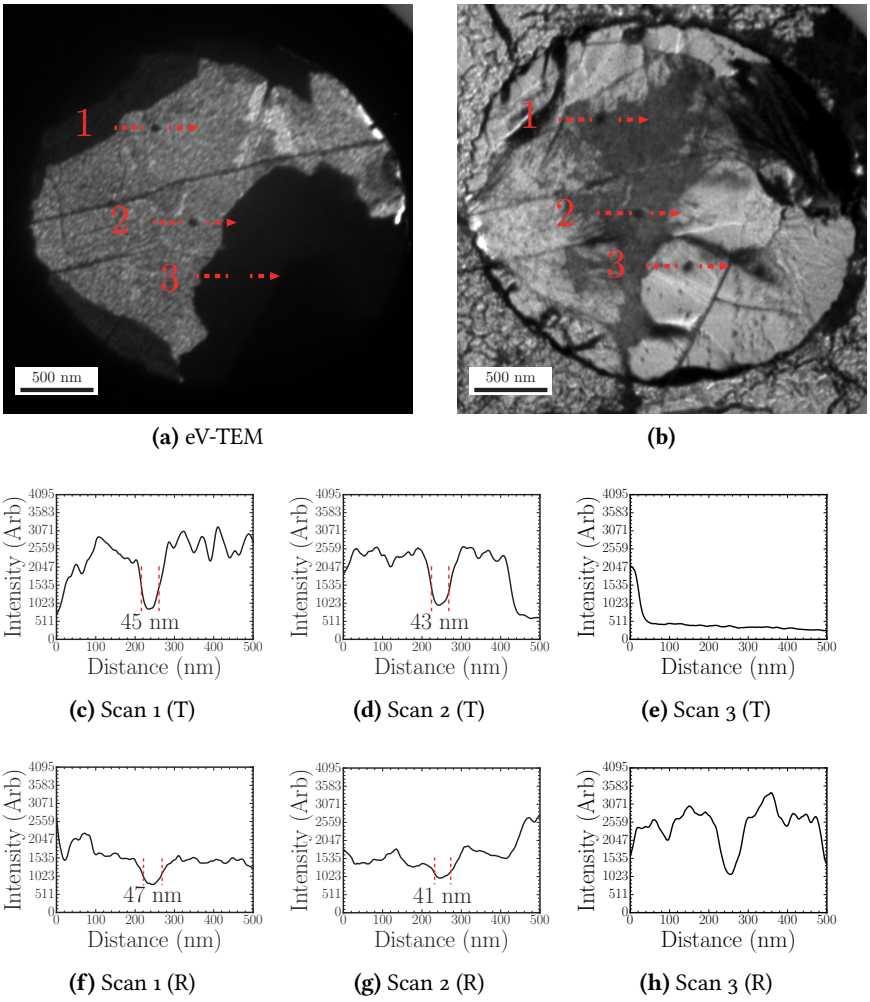

(a) eV-TEM **(b)**

(c) Scan 1 (T) **(d)** Scan 2 (T) **(e)** Scan 3 (T)

(f) Scan 1 (R) **(g)** Scan 2 (R) **(h)** Scan 3 (R)

Figure 3.5: (a),(b): eV-TEM and reflection micrograph from graphene with deposited gold nanoparticles. Immediately after the deposition surface contaminations prevented imaging of the sample with low-energy electrons. After heating this became possible. The nanoparticles coalesce at elevated temperatures. The dots are clusters of AuNPs. **(c)-(e)**: Intensity line scans over the features indicated by arrows 1, 2 and 3 in the eV-TEM micrograph. **(f)-(h)**: Intensity line scans in the reflection micrograph.

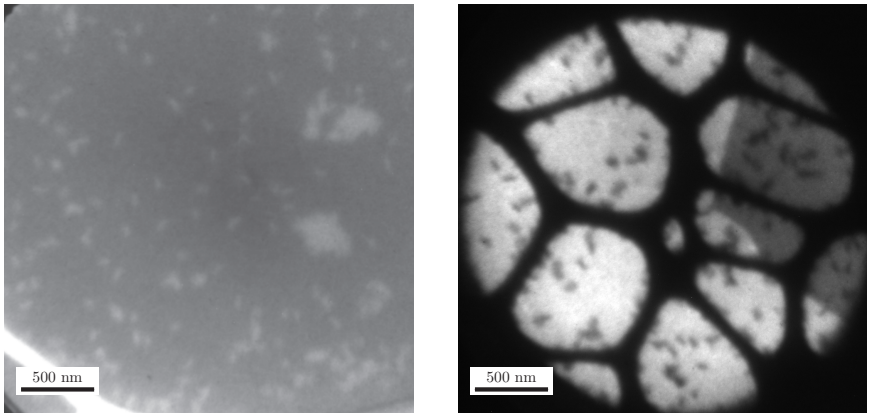

(a) **(b)**

Figure 3.6: Micrographs of DNA origami on graphene oxide. **(a)** Reflection micrograph, obtained with an electron energy of 3 eV, the lighter dots in the figure are DNA origami patches (this is a region with supported graphene oxide). **(b)** eV-TEM micrograph of the DNA origami obtained with an electron energy of 2.1 eV (freestanding graphene oxide).

reflection and is therefore not caused by a particle on the sample. We find that the dots in scans 1 and 2 have a diameter of approximately 40 nm and 45 nm. This is much larger than the individual NP diameter of 10 nm (see figure 2.18). The nanoparticles have coalesced into larger clusters, as a consequence of sample heating.

Even though we do not actually image the nanoparticles in transmission (we only see a shadow), this is a very important step. These results demonstrate the use of graphene as a substrate for nanomaterials. eV-TEM can therefore be used in a much larger range of applications than just the study of two-dimensional materials. Imaging of nanoscale objects is not trivial as heating of the sample is not always a possibility, especially for biological materials which are sensitive to high temperature. In the next section we show that these problems can be overcome and we present eV-TEM micrographs of DNA origami on graphene oxide.

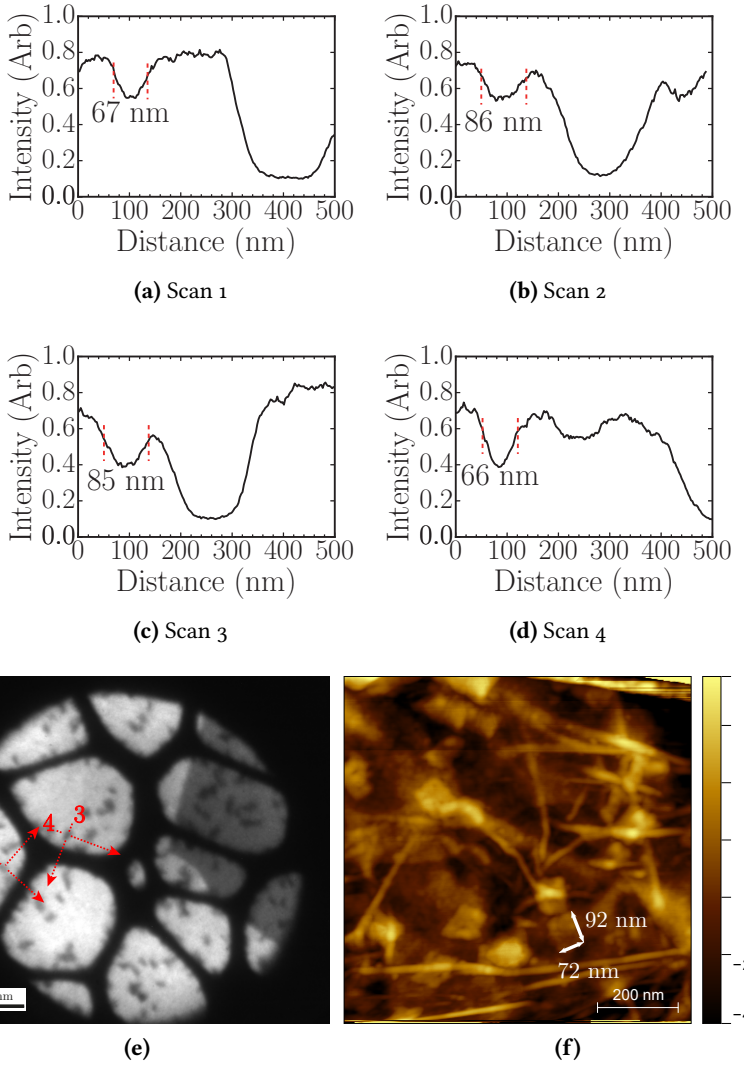

(a) Scan 1 **(b)** Scan 2

(c) Scan 3 **(d)** Scan 4

(e) **(f)**

Figure 3.7: (a)-(d) Line scans of the DNA in the eV-TEM micrograph from the positions indicated in **(e)**. We find that the rectangular patches have a width and length of roughly 70 and 90 nm. This corresponds to what we find with AFM, presented in **(f)** for comparison. It can also be seen (from (a)-(d)) that the transmissivity of the DNA is not zero. eV-TEM can therefore be used to obtain spectroscopic information of DNA.

3.2.2 DNA origami

To image DNA origami we deposited an aqueous solution with the DNA on hydrophilic graphene oxide (as explained in section 2.3.3). Again, proper imaging immediately after loading the sample in the instrument, was impossible. Since graphene oxide is hydrophilic, a thin water layer will be present on the surface. This prevents proper imaging with low energy electrons. With DNA on the sample, heating is not an option; DNA origami will disintegrate at the temperature we use in the gold nanoparticle experiment. However, instead of heating the sample it can be kept in the vacuum of the instrument for a few days. During this time the water evaporates from the surface, enabling imaging with low energy electrons. Figure 3.6a shows a reflection micrograph of DNA origami on graphene oxide. The DNA origami appears as rectangular patches on the graphene oxide substrate. An eV-TEM micrograph of the DNA origami on freestanding graphene oxide is presented in figure 3.7a. Only the suspended graphene oxide is visible in the transmission micrograph. Two different layer thicknesses can be identified from the contrast between the large bright area and the smaller darker area on the right. The web-like structure is again lacey carbon that lies on top of the graphene oxide. The lacey carbon is much thicker than the graphene oxide (about 70 nm, determined from AFM measurements) and transmits very few electrons. Figure 3.7a-d shows line scans of the intensity in the eV-TEM micrograph (figure 3.7e). These line scans run over the DNA origami and over the lacey carbon. This shows that electrons are transmitted through the DNA; the DNA electron transmission is significantly higher than that of lacey carbon. The scan show that the patches have a width and length of approximately 70 nm and 90 nm, in good agreement with the specified size.

This is another very important step that demonstrates imaging of biological nanoscale objects with very low energy electrons. Additionally, we show that graphene oxide can be used as an eV-TEM substrate. Leaving a hydrophobic sample for a long time in the UHV to remove the thin water layer, can be used as an alternative to heating. Having access to both hydrophobic (graphene) and hydrophilic (graphene oxide) substrates enables the study of a wide variety of materials in eV-TEM. Even though at this moment the resolution is not very

impressive, the current methods should allow for spectroscopic measurements on these samples. We expect that better sample preparation methods will improve the imaging resolution. The theoretical resolution limit of eV-TEM is discussed in the next section.

3.3 Resolution of eV-TEM

The resolution of an aberration free imaging system is given by the Rayleigh resolution criterion:

$$R = \frac{0.61\lambda}{\sin(\alpha)} \tag{3.1}$$

where λ is the electron wavelength and α the angle acceptance of the imaging system. The ultimate resolution is therefore achieved for $\alpha \to \frac{\pi}{2}$. However, lenses in an electron optical system are never aberration free and spherical and chromatic aberrations increase with α. A simple expression for the resolution, not taking into account the wave-optical nature of the image-forming process, can be written as follows for small α such that $\sin(\alpha) \to \alpha$ [3, 4]:

$$\delta = \sqrt{\begin{aligned}&\left(\frac{0.61\lambda}{\alpha}\right)^2 + \left(C_3\alpha^3\right)^2 + \left(C_5\alpha^5\right)^2 \\ &+ \left(\frac{\Delta E}{E}\right)^2 \left[(C_c\alpha)^2 + \left(C_{C3}\alpha^3\right)^2\right] + \left(\frac{\Delta E}{E}\right)^4 (C_{CC}\alpha)^2\end{aligned}} \tag{3.2}$$

The first term is the Rayleigh resolution limit that decreases with α. The aberrations are given by an aberration coefficient and an α. The third order spherical aberration is given by C_3 and the second rank chromatic aberration coefficient by C_C. The chromatic aberrations scale with the electron energy and energy width as $\frac{\Delta E}{E}$. To reach the optimal resolution of the microscope, a trade-off has to be made between the Rayleigh diffraction limit and the aberrations. Sebastian Schramm has shown in his thesis how to do this more accurately [4]. In the ESCHER setup the aberrations of the objective lens can be corrected with the aberration correcting mirror optics. In figure 3.8b equation 3.2 is plotted in the corrected and uncorrected cases for imaging in reflection. The coefficients are taken from [3] for 3 eV electrons. The angle acceptance can be limited by a contrast aperture to optimize α. In figure 3.8a

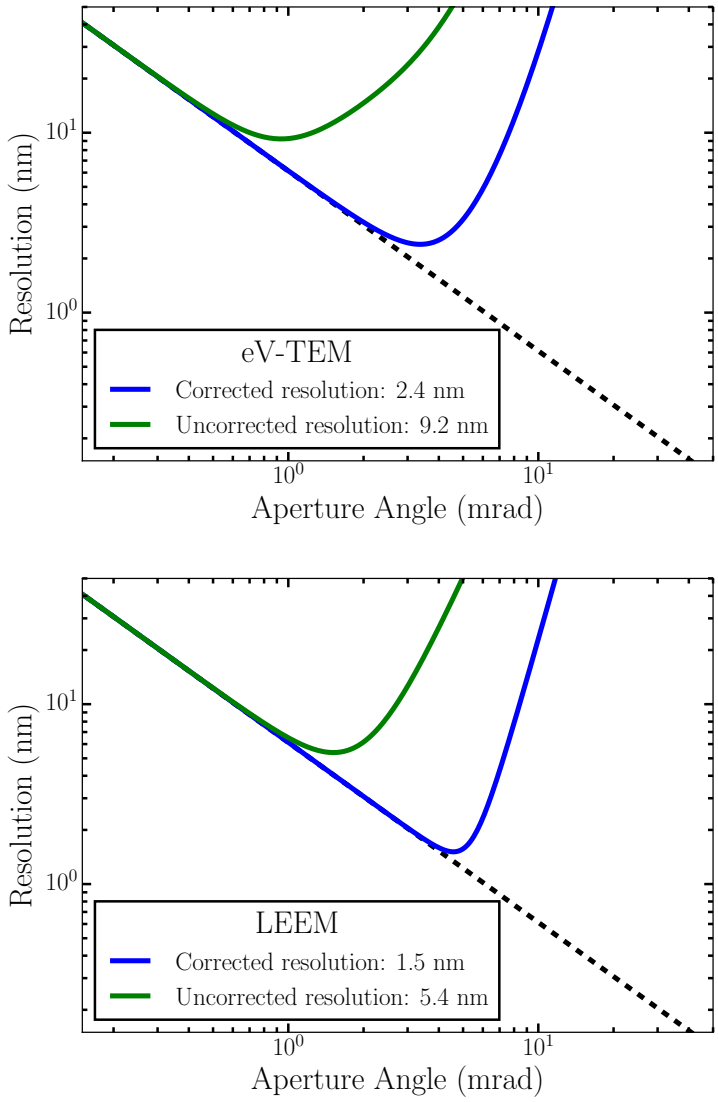

Figure 3.8: Resolution as a function of angular acceptance with the small angle approximation calculated with equation 3.2 using the aberration coefficients of [3]. We use the same coefficients for eV-TEM and LEEM, the only difference is the energy spread, ΔE; 0.25 eV for reflection and 0.8 eV in eV-TEM. In LEEM this leads to resolution of the uncorrected system of 5.4 nm and 1.5 nm for the corrected system. In eV-TEM the resolution becomes 9.2 nm for the uncorrected system and 2.4 nm for the aberration corrected system.

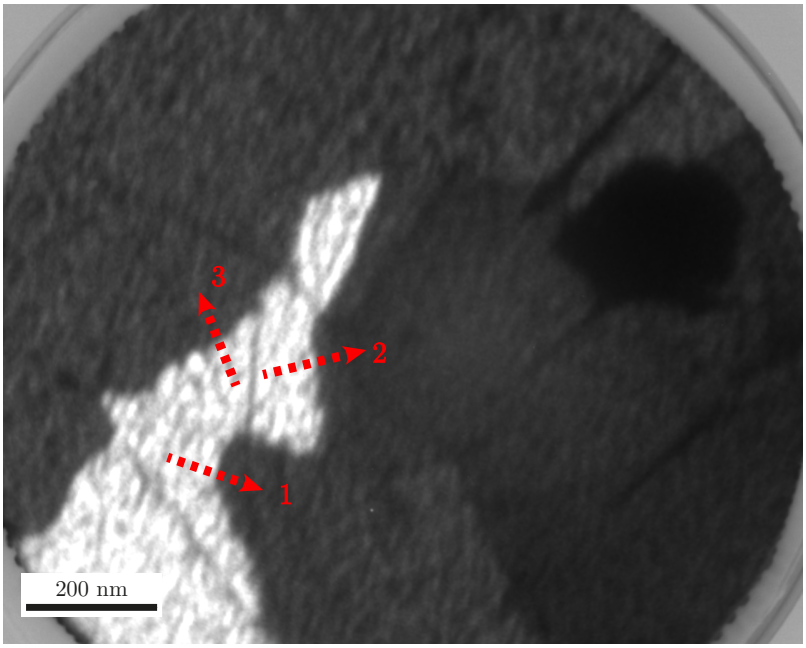

(a)

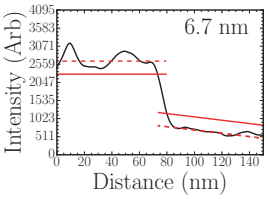

(b) Scan 1

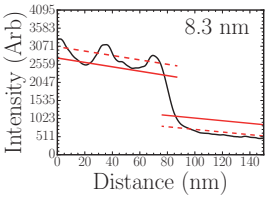

(c) Scan 2

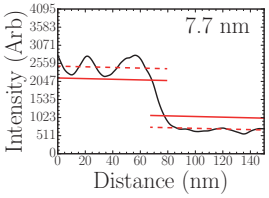

(d) Scan 3

Figure 3.9: eV-TEM resolution determined on multilayer graphene in **(a)**. **(b)**-**(d)** Line scans in (a) indicated by numbers.

the resolution for transmission imaging is shown. Since in transmission mode the same imaging system is used as for reflection, the same aberration coefficients are used. Only ΔE is different because different electrons sources are used. For transmission we use $\Delta E = 0.8$ eV and for reflection 0.25 eV.

In figure 3.9 we determine the resolution of an eV-TEM micrograph (the graphene is suspended on a molybdenum coated Si_3N_4 window). Figures 3.9b-3.9d show intensity line scans from positions in the micrograph, indicated in figure 3.9a. These are all on the boundary between two regions with a different layer number. The resolution is determined to be the distance over which the intensity increases from 20 % to 80 %, as described in [4]. The aberration correction and the aperture diameter (i.e. α) have not been optimized [3]. Under these circumstances the resolution is between 6.7 nm and 8.3 nm. This is somewhat better than expected for an uncorrected system, but not as good as expected for an optimized corrected system. We expect that improvements in sample alignment and optimization of the electron mirror settings will be able to further improve resolution to the 2-3 nm level.

3.4 Outlook

The results presented in this chapter are very promising and suggest that it is possible to do quantitative spectroscopic experiments on biological materials with low-energy electrons. Many improvements can still be made as the imaging conditions are not yet ideal. The sample preparation we used to deposit nanoscale objects on the substrates is very straightforward but does not allow for the ultra clean conditions necessary for high resolution imaging. Longchamp et al. demonstrated a method in which they prepare ultra clean graphene (with the same method we used) in the vacuum and afterwards introduce proteins in situ by depositing them on the graphene with a method called soft landing electro spray [5, 6]. We expect that with better sample preparation methods it will become possible to improve the resolution significantly when imaging biological materials. Longchamp et al. used this method to prepare proteins to be imaged with low-energy electron holography [5]. This is a very interesting technique as it as is does not require any optical elements between the sample and detector that would otherwise introduce aberrations. A drawback of this approach, however, is that no distinction can be made between inelastically scattered and secondary electrons. In the

diffraction pattern, presented in figure 3.4, we observe a significant secondary electron emission. It would be worthwhile to investigate how to install a highly coherent electron source in the eV-TEM sample holder as this should allow for energy-filtered holographic spectroscopy of single proteins as well as real space elastic and inelastic imaging. Even the limited space of the sample cap is sufficient for such a source, leaving much room for further development.

References

1. Kaiser U. *et al.* Transmission electron microscopy at 20kV for imaging and spectroscopy. *Ultramicroscopy* **111,** 1239–1246 (2011).
2. Locatelli A., Knox K. R., Cvetko D., Menteş T. O., Niño M. A., Wang S., Yilmaz M. B., Kim P., Osgood R. M. & Morgante A. Corrugation in Exfoliated Graphene: An Electron Microscopy and Diffraction Study. *ACS Nano* **4,** 4879–4889 (2010).
3. Tromp R., Hannon J., Ellis A., Wan W., Berghaus A. & Schaff O. A new aberration-corrected, energy-filtered LEEM/PEEM instrument. I. Principles and design. *Ultramicroscopy* **110,** 852–861 (2010).
4. Schramm S. M. *Imaging with Aberration-Corrected Low Energy Electron Microscopy* PhD thesis (2013). ISBN: 9789085931522.
5. Longchamp J.-N., Rauschenbach S., Abb S., Escher C., Latychevskaia T., Kern K. & Fink H.-W. Imaging proteins at the single-molecule level. *Proceedings of the National Academy of Sciences* **114,** 1474–1479 (2017).
6. Longchamp J.-n., Rauschenbach S., Abb S., Escher C., Latychevskaia T., Kern K. & Fink H.-W. Imaging proteins at the single-molecule level. *Proceedings of the National Academy of Sciences* **114,** 1474–1479 (2017).